*Sensors and Materials*, Vol. 34, No. 6 (2022) 2075–2087
MYU Tokyo



LETTER

S & M 2957

# Foot-mounted Dual-sensor Single-board Pedestrian Inertial Navigation System Based on Position and Velocity Constraints

Shao Chen,[1] Zhenchun Lu,[1] Xiangbo Xu,[1*] Jinhao Liu,[1**] and Zhongwei Bi[2]

[1]School of Technology, Beijing Forestry University,
No. 35 Qinghua East Road, Haidian District, Beijing 100083, China
[2]Beijing High Speed Suspension Power Technology Co., Ltd.,
4th Binhe Road, Qinghe East, Haidian District, Beijing 100085, China

(Received February 16, 2022; accepted March 30, 2022)

***Keywords:*** pedestrian positioning, inertial sensors, zero velocity update, velocity and position constraint, Kalman filter

Pedestrian inertial navigation systems (PINSs) based on zero velocity update (ZUPT) are extensively used in pedestrian positioning. However, because of sensor drift, traditional foot-mounted PINSs show poor precision. We design a dual MIMU single-board PINS and propose a new constraint method. A constant three-dimensional (3D) position difference constraint can be formed on the basis of the layout of the two sensors on the circuit board. The constraints of (linear) velocity, angular velocity, and constant position difference are constructed on the basis of the Coriolis theorem. To obtain the optimal velocity and position, a linear Kalman filter is constructed. Rectangle and stair experiments are performed to verify the proposed method. The results show that the proposed method can improve the positioning accuracy compared with the classical ZUPT and dual-sensor foot-to-foot constraint methods. Compared with the constraint in the two-step maximum distance scheme, the proposed position and velocity constraints are clearer and can be applied to the whole gait phase. Furthermore, the proposed PINS in this study has the advantages of easy installation, small size, high-speed communications, and low power consumption.

## 1. Introduction

With the rapid development of location-based services, real-time accurate location algorithms have attracted extensive attention. Common positioning techniques include the Global Positioning System (GPS), WiFi positioning, Bluetooth positioning, RF identification positioning, and inertial navigation systems (INSs).[1–4] INSs, with their advantages of no information exchange, low cost, and robustness against interference, are widely used for positioning in forests, underground mines, and underwater, i.e., locations beyond the reach of base station communication signals or where the GPS signal is weak. The maturity of MEMS-based inertial technology enables the possibility of wearable PINS.[5]

*Corresponding author: e-mail: xuxiangbo@bjfu.edu.cn
**Corresponding author: e-mail: liujinhao@bjfu.edu.cn
https://doi.org/10.18494/SAM3853

ISSN 0914-4935 
https://myukk.org/

However, because of sensor drift and integral error, the positioning error of PINS will diverge rapidly over time. Considerable research has been carried out on suppressing the divergence of PINS error. Zero velocity update (ZUPT) is the most commonly used method for suppressing divergence. ZUPT divides the pedestrian walking gait into the stance phase and swing phase. It corrects the navigation error by assuming that the theoretical velocity is zero during the stance phase.[6] The performance of ZUPT detectors has been well studied because of the importance of the stance phase. In conventional methods, the standing phase is judged using the thresholds of acceleration and angular velocity in the sliding window. On the basis of such conventional pedestrian gait detection methods, Tian *et al.* added the acceleration variance threshold in the sliding window to reduce the misjudgment caused by noise.[7] Zhao and Jalal proposed a double-order ZUPT detector, in which the conventional threshold judgment is combined with a time threshold. The accuracy of this detector was improved by identifying the pseudo-stance phase and preventing premature detection.[8] Many correction methods based on the stance phase have been proposed. Zheng *et al.* designed a Kalman filter for estimating the state error of a system, and the estimated result was used for compensation to improve the accuracy of positioning.[9] Wang *et al.* designed a Kalman filter model based on multiple sensors.[10] In their model, the velocity and angular velocity were set to zero to reduce the accumulated error during the stance phase, and a magnetometer and barometer were employed to correct the heading and altitude, respectively. Hsu *et al.* proposed a method based on a double-stage quaternion-based extended Kalman filter (EKF) to suppress cumulative error.[11] The double-stage EKF ensured that the data obtained from the accelerometer and magnetometer did not interfere with each other. Although the heading can be observed with the magnetometer, the heading error still cannot be ignored because the magnetic field is easily disturbed. Furthermore, correction methods based on ZUPT can only be used in the stance phase, and there is no correction in the swing phase, which accounts for the majority of the pedestrian gait. Thus, the performance of ZUPT based on a single low-cost noisy inertial measurement unit (IMU) is unsatisfactory.

To improve the ZUPT algorithm based on a single IMU, multi-IMU pedestrian navigation algorithms have been widely studied. Skog *et al.* designed a printed circuit board with 18 IMUs and showed that the mean value of the positioning results of each IMU in the IMU array is effective to improve the positioning accuracy.[12] Bose *et al.* verified that the noise performance of an IMU array is superior to that of a single IMU.[13] Liu *et al.* designed an IMU array that reduced the temperature drift of a gyroscope and improved the navigation accuracy.[14] However, these methods based on an IMU array involved simple averaging without any consideration of the constraints between IMUs in the IMU array. Too many IMUs will result in an excessively large circuit board, decreased wearability, and reduced sampling and calculation frequencies of the IMU array. Thus, dual-IMU schemes have been studied more extensively than multi-IMU schemes. Shi *et al.* proposed a dynamic ellipsoid constraint to improve positioning accuracy.[15] The pedestrian step size will not exceed the maximum step size, so the pedestrian single-step position increment is limited to a circle having a radius of the maximum step size. The maximum step size is used to constrain the divergence of the 2D horizontal plane positioning error. Similarly, a parameter related to the leg length is used as the radius of another circle to constrain the divergence of the height error calculated by PINS. Niu *et al.* proposed a method to improve

positioning accuracy based on minimum foot-to-foot distance.[16] Zhao *et al.* analyzed dual-gait kinetics to detect the stance phase and designed an inverted pendulum model to constrain positioning error. The drift of the heading was effectively reduced in their model.[17] Li *et al.* formulated a foot-to-foot inequality constraint[18] that can suppress the divergence of navigation. However, these studies are still concerned with only the stance phase. Furthermore, the constraints were not constant and needed to be adjusted in accordance with the actual situation. Wang *et al.* proposed an adaptive inequality constraint.[19] They assumed that the distance between two feet when one foot is in the initial stance phase and the other is at the end of the stance phase is related to the motion. Two ultrasonic sensors were used to establish the distance constraint between two feet.[20] This method proposed by Wang *et al.* first calculates the position of one foot through ZUPT, then the position of the other foot is constrained by the distance measured by ultrasound. Although this is a clear constraint, the complexity of the hardware is increased, making it difficult to wear for pedestrians. Moreover, the dynamic performance of ultrasonic ranging is poor. The precision of navigation and the wearability of the device based on the foot-to-foot constraints are still unsatisfactory.

In this study, we developed a new PINS with two 9-axis sensors composed of a magnetometer and IMU (MIMU) to restrict the divergence of positioning error in the whole process of pedestrian movement instead of only in the stance phase. The PINS is worn on a shoe. The relative spatial position of the two MIMUs is constant, and this can be used as a position constraint. Because the PINS placed on the foot has angular velocity with the movement of the pedestrian, the velocities calculated by the two MIMUs are related to the angular velocity and position difference. This relationship can be used as a velocity constraint. The above position and velocity constraints are clear and effective in both the stance phase and the swing phase without the need to employ additional sensors. Adding a MIMU to a classical single MIMU circuit board only nominally increases the size of the circuit board. Such a small PINS is convenient for pedestrians to wear. Moreover, the sampling frequency of the dual MIMU based on a serial peripheral interface (SPI) can meet the requirements of PINSs.

This paper is organized as follows. We present the theory of system modeling in Sect. 2. In Sect. 3, we describe our design of the Kalman filter. In Sect. 4, the experiment is introduced and an analysis of the experimental results is given. Finally, a summary of this work is given in Sect. 5.

## 2. Theory of System Modeling

In this study, a circuit board with two low-cost MIMUs is tightly fixed onto a shoe, as shown in Fig. 1. The navigation frame $n$ is defined as the east-north-sky geographic coordinate system. The $x$–$y$–$z$ axes of the two body frames $b_i$ ($i$ = 1, 2) correspond to the right-front-up axes of the sensors. In this study, the unit quaternion $\boldsymbol{q}_i$ is used to represent the rotation of frame $n$ to frame $b_i$, and the mathematical expression for $\boldsymbol{q}_i$ is

$$\boldsymbol{q}_i = \cos\left(\frac{\theta_i}{2}\right) + \boldsymbol{u}_i \sin\left(\frac{\theta_i}{2}\right), \tag{1}$$

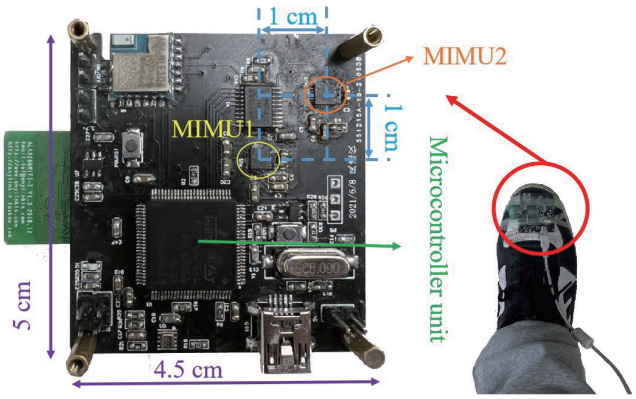


Fig. 1. (Color online) Foot-mounted circuit board with two MIMUs.

where $\boldsymbol{u}_i$ is the unit vector of the rotation axis in frame $n$, and $\theta_i$ is the angle of rotation.

$$\begin{aligned} \boldsymbol{q}_i &= \begin{bmatrix} q_{0|i} & q_{1|i} & q_{2|i} & q_{3|i} \end{bmatrix}^T \\ q_{0|i} &= \cos\left(\frac{\theta_i}{2}\right) \\ \begin{bmatrix} q_{1|i} & q_{2|i} & q_{3|i} \end{bmatrix}^T &= \boldsymbol{u}_i \sin\left(\frac{\theta_i}{2}\right) \end{aligned} \tag{2}$$

Vector $\boldsymbol{v}_i$ in frame $b_i$ and vector $\boldsymbol{y}$ in frame $n$ satisfy[22]

$$\boldsymbol{v}_i = \boldsymbol{R}_n^{b_i} \boldsymbol{y}, \tag{3}$$

where $\boldsymbol{R}_n^{b_i}$ is the rotation matrix for converting frame $n$ to frame $b_i$, and its mathematical expression is[23]

$$\boldsymbol{R}_n^{b_i} = \left(\boldsymbol{R}_{b_i}^n\right)^T = \begin{bmatrix} q_{0|i}^2 + q_{1|i}^2 - q_{2|i}^2 - q_{3|i}^2 & 2\left(q_{1|i}q_{2|i} + q_{0|i}q_{3|i}\right) & 2\left(q_{1|i}q_{3|i} - q_{0|i}q_{2|i}\right) \\ 2\left(q_{1|i}q_{2|i} - q_{0|i}q_{3|i}\right) & q_{0|i}^2 - q_{1|i}^2 + q_{2|i}^2 - q_{3|i}^2 & 2\left(q_{0|i}q_{1|i} + q_{2|i}q_{3|i}\right) \\ 2\left(q_{1|i}q_{3|i} + q_{0|i}q_{2|i}\right) & 2\left(q_{2|i}q_{3|i} - q_{0|i}q_{1|i}\right) & q_{0|i}^2 - q_{1|i}^2 - q_{2|i}^2 + q_{3|i}^2 \end{bmatrix}. \tag{4}$$

As shown in Fig. 2, the vector relationship in frame $b_i$ or frame $n$ at any time can be expressed as

$$\boldsymbol{m} = \boldsymbol{r}_2 - \boldsymbol{r}_1, \tag{5}$$

where $\boldsymbol{r}_i$ is the position vector of MIMU$_i$. $\boldsymbol{m}$ is the relative position vector of two MIMUs. The discrete equations of $\boldsymbol{v}_i$ and $\boldsymbol{r}_i$ in frame $n$ are given as

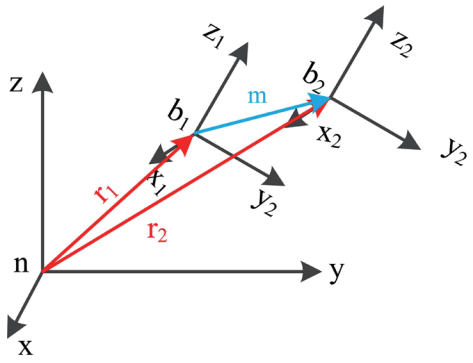


Fig. 2. (Color online) Vector relationship in frame $n$ or $b_i$.

$$\begin{cases} \boldsymbol{v}_{i|k}^{n} = \boldsymbol{v}_{i|k-1}^{n} + (\boldsymbol{R}_{b_i}^{n}\boldsymbol{a}_{k}^{b_i} - \boldsymbol{g}^{n})\Delta t, \\ \boldsymbol{r}_{i|k}^{n} = \boldsymbol{r}_{i|k-1}^{n} + \boldsymbol{v}_{i|k-1}^{n}\Delta t + \dfrac{1}{2}(\boldsymbol{R}_{b_i}^{n}\boldsymbol{a}_{k}^{b_i} - \boldsymbol{g}^{n})\Delta t^{2}, \end{cases} \tag{6}$$

where $\boldsymbol{a}_k^{b_i}$ is the acceleration value measured by MIMU$_i$ at time $k$, $\boldsymbol{g}^n = [0, 0, 9.8]^T$ is the gravitation vector, $\Delta t$ is the sampling time, and $\boldsymbol{v}_{i|k}^n$ and $\boldsymbol{r}_{i|k}^n$ are the velocity and position of MIMU$_i$ in frame $n$ at time $k$, respectively.

Applying the Coriolis theorem,[23] we obtain

$$\left.\frac{d\boldsymbol{r}_i}{dt}\right|_n = \left.\frac{d\boldsymbol{r}_i}{dt}\right|_{b_i} + \boldsymbol{w}_{nb_i} \times \boldsymbol{r}_i. \tag{7}$$

This can be written in frame $n$ as

$$\boldsymbol{v}_i^n = R_{b_i}^n \boldsymbol{v}_i^{b_i} + w_{nb_i}^n \times r_i^n, \tag{8}$$

where $\boldsymbol{w}_{nb_i}^n$ is the angular velocity of frame $b_i$ relative to frame $n$ in frame $n$. Because the two MIMUs are carrier-fixed, $\boldsymbol{w}_{nb_1}^n = \boldsymbol{w}_{nb_2}^n$. $\boldsymbol{v}_{bij}$ is the velocity of MIMU$_i$ in frame $b_i$. Clearly, $\boldsymbol{v}_{bij} = 0$. Thus, we obtain

$$\boldsymbol{v}_i^n = \boldsymbol{w}_{nb_i}^n \times \boldsymbol{r}_i^n. \tag{9}$$

From Eqs. (5) and (9), the velocity difference of two MIMUs can be calculated as

$$\boldsymbol{v}_2^n - \boldsymbol{v}_1^n = \boldsymbol{w}_{nb_2}^n \times \boldsymbol{r}_2^n - \boldsymbol{w}_{nb_1}^n \times \boldsymbol{r}_1^n = \boldsymbol{w}_{nb_1}^n \times \boldsymbol{m}^n. \tag{10}$$

From Eq. (3), we obtain

$$\boldsymbol{m}^{n} = \boldsymbol{R}_{b_1}^{n}\boldsymbol{m}^{b_1},\ \boldsymbol{w}_{nb_1}^{n} = \boldsymbol{R}_{b_1}^{n}\boldsymbol{w}_{nb_1}^{b_1}. \tag{11}$$

Substituting Eq. (11) into Eq. (5) yields

$$\boldsymbol{r}_2^{n} - \boldsymbol{r}_1^{n} = \boldsymbol{R}_{b_1}^{n}\boldsymbol{m}^{b_1}. \tag{12}$$

Substituting Eq. (11) into Eq. (10) yields

$$\boldsymbol{v}_2^{n} - \boldsymbol{v}_1^{n} = \boldsymbol{R}_{b_1}^{n}\boldsymbol{w}_{nb_1}^{b_1} \times \boldsymbol{R}_{b_1}^{n}\boldsymbol{m}^{b_1}, \tag{13}$$

where $\boldsymbol{w}_{nb_1}^{b_1}$ is the angular velocity of frame $b_1$ relative to frame $n$ in frame $b_1$; this is the angular velocity measured by MIMU$_1$. Since $\boldsymbol{w}_{nb_1}^{n} = \boldsymbol{w}_{nb_2}^{n}$, we can use the average value of the measured $\boldsymbol{w}_{nb_1}^{n}$ and $\boldsymbol{w}_{nb_2}^{n}$ to improve the precision of the low-cost sensors. $\boldsymbol{m}^{b_1}$ is the relative position vector of two MIMUs in frame $b_1$, and $\boldsymbol{m}^{b_1} = [0.01 \quad 0.01 \quad 0]^{T}$.

## 3. Design of Linear Discrete Kalman Filter

$\boldsymbol{R}_{b_1}^{n}$ in Eqs. (12) and (13) updated by the gyroscope contains gyroscope noise. Therefore, the terms on the right sides of Eqs. (12) and (13) can be regarded as data measured by a sensor. The ability to fuse the data of various sensors to obtain the optimal estimation is the advantage of using the Kalman filter. Hence, the discrete Kalman filter is designed.

The standard formula of the Kalman filter is[24]

$$\boldsymbol{x}(k) = \boldsymbol{F}\boldsymbol{x}(k-1) + \boldsymbol{B}\boldsymbol{u}(k), \tag{14}$$

$$\boldsymbol{Z}(k) = \boldsymbol{H}\boldsymbol{x}(k). \tag{15}$$

Equation (14) is called the state equation, and it describes the evolution process of the system state. In this study, the velocity and position calculated by the two MIMUs are selected to obtain the state variable $\boldsymbol{x}$.

$$\boldsymbol{x} = \begin{bmatrix} \boldsymbol{r}_1^{n} & \boldsymbol{r}_2^{n} & \boldsymbol{v}_1^{n} & \boldsymbol{v}_2^{n} \end{bmatrix} \tag{16}$$

Here, $\boldsymbol{r}_i^{n}$ and $\boldsymbol{v}_i^{n}$ are the position vector and velocity vector of MIMU$_i$ in frame $n$, respectively. From Eq. (6), we obtain the state transition matrix $\boldsymbol{F}$, input vector $\boldsymbol{u}$, and control matrix $\boldsymbol{B}$.

$$\boldsymbol{F} = \begin{bmatrix} \boldsymbol{I}_{3\times3} & \boldsymbol{0}_{3\times3} & \Delta t * \boldsymbol{I}_{3\times3} & \boldsymbol{0}_{3\times3} \\ \boldsymbol{0}_{3\times3} & \boldsymbol{I}_{3\times3} & \boldsymbol{0}_{3\times3} & \Delta t * \boldsymbol{I}_{3\times3} \\ \boldsymbol{0}_{3\times3} & \boldsymbol{0}_{3\times3} & \boldsymbol{I}_{3\times3} & \boldsymbol{0}_{3\times3} \\ \boldsymbol{0}_{3\times3} & \boldsymbol{0}_{3\times3} & \boldsymbol{0}_{3\times3} & \boldsymbol{I}_{3\times3} \end{bmatrix},\ \boldsymbol{u}(k) = \begin{bmatrix} \boldsymbol{R}_{b_1}^{n}\boldsymbol{a}_k^{b_1} - \boldsymbol{g}^{n} \\ \boldsymbol{R}_{b_2}^{n}\boldsymbol{a}_k^{b_2} - \boldsymbol{g}^{n} \end{bmatrix},\ \boldsymbol{B} = \begin{bmatrix} \frac{\Delta t^2}{2} * \boldsymbol{I}_{3\times3} & \boldsymbol{0}_{3\times3} \\ \boldsymbol{0}_{3\times3} & \frac{\Delta t^2}{2} * \boldsymbol{I}_{3\times3} \\ \Delta t * \boldsymbol{I}_{3\times3} & \boldsymbol{0}_{3\times3} \\ \boldsymbol{0}_{3\times3} & \Delta t * \boldsymbol{I}_{3\times3} \end{bmatrix} \tag{17}$$

Equation (15) is called the observation equation. In this work, there are two observation equations because of the difference in pedestrian gait. From Eqs. (12) and (13), we obtain the observation equation in the swing phase as

$$\boldsymbol{Z}_1 = \boldsymbol{H}_1\boldsymbol{x}(k),\ \boldsymbol{Z}_1 = \begin{bmatrix} \boldsymbol{R}_{b_1}^{n}\boldsymbol{w}_{nb_1}^{b_1} \times \boldsymbol{R}_{b_1}^{n}\boldsymbol{m}^{b_1} \\ \boldsymbol{R}_{b_1}^{n}\boldsymbol{m}^{b_1} \end{bmatrix},\ \boldsymbol{H}_1 = \begin{bmatrix} \boldsymbol{0}_{3\times3} & \boldsymbol{0}_{3\times3} & -\boldsymbol{I}_{3\times3} & \boldsymbol{I}_{3\times3} \\ -\boldsymbol{I}_{3\times3} & \boldsymbol{I}_{3\times3} & \boldsymbol{0}_{3\times3} & \boldsymbol{0}_{3\times3} \end{bmatrix}, \tag{18}$$

where $\boldsymbol{Z}_1$ and $\boldsymbol{H}_1$ are the observation vector and the observation matrix in the swing phase, respectively.

In the stance phase, during which the velocities should be zero, the observation equation is

$$\boldsymbol{Z}_2 = \boldsymbol{H}_2\boldsymbol{x}(k),\ \boldsymbol{Z}_2 = \begin{bmatrix} \boldsymbol{R}_{b_1}^{n}\boldsymbol{w}_{nb_1}^{b_1} \times \boldsymbol{R}_{b_1}^{n}\boldsymbol{m}^{b_1} \\ \boldsymbol{R}_{b_1}^{n}\boldsymbol{m}^{b_1} \\ \boldsymbol{0}_{3\times1} \\ \boldsymbol{0}_{3\times1} \end{bmatrix},\ \boldsymbol{H}_2 = \begin{bmatrix} \boldsymbol{0}_{3\times3} & \boldsymbol{0}_{3\times3} & -\boldsymbol{I}_{3\times3} & \boldsymbol{I}_{3\times3} \\ -\boldsymbol{I}_{3\times3} & \boldsymbol{I}_{3\times3} & \boldsymbol{0}_{3\times3} & \boldsymbol{0}_{3\times3} \\ \boldsymbol{0}_{3\times3} & \boldsymbol{0}_{3\times3} & \boldsymbol{I}_{3\times3} & \boldsymbol{0}_{3\times3} \\ \boldsymbol{0}_{3\times3} & \boldsymbol{0}_{3\times3} & \boldsymbol{0}_{3\times3} & \boldsymbol{I}_{3\times3} \end{bmatrix}, \tag{19}$$

where $\boldsymbol{Z}_2$ and $\boldsymbol{H}_2$ are the observation vector and the observation matrix in the stance phase, respectively. The state variable $\boldsymbol{x}$ estimated using Eq. (14) is corrected using Eqs. (18) and (19) and the correction equation is

$$\boldsymbol{x}_{best}(k) = \boldsymbol{x} + \boldsymbol{K}_i(k)(\boldsymbol{Z}_i(k) - \boldsymbol{H}_i\boldsymbol{x}(k)), \tag{20}$$

where $\boldsymbol{x}_{best}$ is the optimal estimate of $\boldsymbol{x}$. $\boldsymbol{K}_i(k)$ is the gain at $k$, which we obtain using

$$\begin{aligned} &\boldsymbol{K}_i(k) = \boldsymbol{P}^{-}(k)\boldsymbol{H}_i^{T}(\boldsymbol{H}_i\boldsymbol{P}^{-}(k)\boldsymbol{H}_i^{T} + \boldsymbol{R}_i(k)), \\ &\boldsymbol{P}^{-}(k) = \boldsymbol{F}\boldsymbol{P}(k-1)\boldsymbol{F}^{T} + \boldsymbol{Q}(k-1), \end{aligned} \tag{21}$$

where $\boldsymbol{P}^{-}(k)$ the state estimation error covariance at time $k$, and it reflects the iterative error of Eq (14). $\boldsymbol{R}_i(k)$ is the observation noise covariance matrix at time $k$. $\boldsymbol{P}(k-1)$ is the optimal estimation error covariance at time $k-1$. $\boldsymbol{Q}(k-1)$ is the process noise covariance matrix.

Finally, $\boldsymbol{P}(k)$ is updated using Eq. (19) to

$$\boldsymbol{P}(k) = (\boldsymbol{I} - \boldsymbol{K}_i(k)\boldsymbol{H}_i)\boldsymbol{P}^{-}(k). \tag{22}$$

The operation process of the PINS is as follows.

(1) Sample the data of dual MIMUs.

(2) Calculate $\boldsymbol{R}_{b_1}^{n}$.

(3) Calculate state estimation $\boldsymbol{x}(k) = \boldsymbol{F}\boldsymbol{x}(k-1) + \boldsymbol{B}\boldsymbol{u}(k)$.

(4) Calculate state estimation error covariance $\boldsymbol{P}^{-}(k) = \boldsymbol{F}\boldsymbol{P}(k-1)\boldsymbol{F}^{T} + \boldsymbol{Q}(k-1)$.

(5) Calculate gain $\boldsymbol{K}_i(k) = \boldsymbol{P}^{-}(k)\boldsymbol{H}_i^{T}(\boldsymbol{H}_i\boldsymbol{P}^{-}(k)\boldsymbol{H}_i^{T} + \boldsymbol{R}_i(k))$.

(6) Calculate optimal state estimation $\boldsymbol{x}_{best}(k) = \boldsymbol{x} + \boldsymbol{K}_i(k)(\boldsymbol{Z}_i(k) - \boldsymbol{H}_i\boldsymbol{x}(k))$.
(7) Calculate optimal estimation error covariance $\boldsymbol{P}(k) = (\boldsymbol{I} - \boldsymbol{K}_i(k)\boldsymbol{H}_i)\boldsymbol{P}^{-}(k)$.

The flowchart of PINS operation is shown in Fig. 3. Figure 3 shows the flow chart of the PINS operation to suppress error divergence throughout the gait cycle in this work. The magnitude of acceleration and angular velocity and the variance of acceleration are used to detect the zero velocity interval (the stance phase).[10]

## 4. Experiments

To demonstrate the effectiveness of the proposed method, two groups of experiments are designed. To verify the proposed method, it is compared with the classical ZUPT algorithm and the foot-to-foot constraint algorithm.[10,22]

### 4.1 Experimental setup

In this study, the low-cost ICM20948 is integrated with a three-axis accelerometer and a three-axis gyroscope. The three-axis accelerometer is used as the MIMU. The details of MIMU are shown in Table 1. STM32F407 is selected as the microcontroller unit. The SPI-based communication ensures few communication lines and high efficiency. Because the linear Kalman filter is established, the calculation load is light, and nonlinear error is avoided, real-time accurate navigation can be realized. The sampling and calculation frequency is 100 Hz.

The MIMU package is 3 × 3 × 1 mm$^3$. Adding an MIMU on a traditional single MIMU circuit board to establish the constraint equations of velocity and position only negligibly increases the volume of the circuit board, making it convenient for pedestrians to wear. The experimental circuit board integrating two MIMUs is mounted at the tip of the shoe, as shown in Fig. 1.

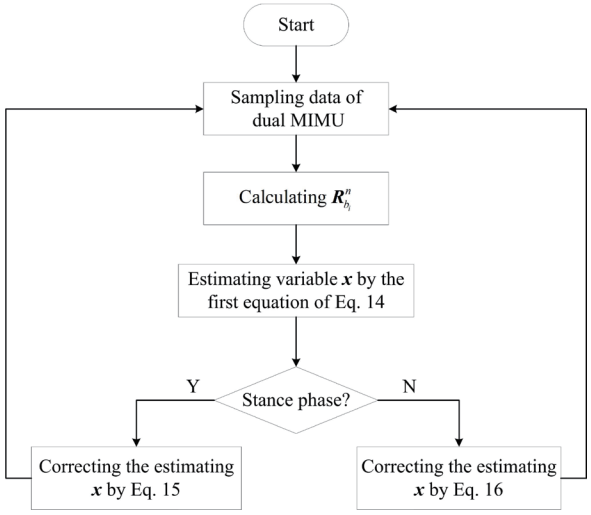


Fig. 3. Flow chart of PINS operation.

Table 1
Detailed indicators of MIMU.

| | Gyroscope (dps) | Accelerometer | Magnetometer (μT) |
|---|---|---|---|
| Full-scale range | ±1000 | ±8 g | ±4900 |
| Initial tolerance | ±5 | ±25 mg | ±300 |

### 4.2 Comparative experiment

The rectangular track and stair experiments were designed. PINS can be mounted on any shoe. As shown in Fig. 1, the right shoe was chosen. The experimenter walked at a normal speed of pedestrians along the lines (1-2-3-4-1) shown in Figs. 4 and 6. PINS collected the angular velocity, acceleration, and magnetic field intensity of the right foot measured by the two MIMUs and transmitted the data to the computer through the serial port. In this study, the velocity and position were obtained by integrating acceleration, and the relationships of velocity constraint and position constraint are fixed, so the experimental results will not change significantly for different wearers. Therefore, experiments are completed by one person.

#### (1) Rectangular track experiment

The experimental site is a rectangular site composed of many square bricks of fixed size, with 30 bricks along the length and 15 bricks along the width. The side length of the square bricks is 0.6 m. Thus, the rectangular site has a length of 18 m and a width of 9 m, as shown in Fig. 4. The results are shown in Fig. 5.

The experimental results show that the maximum position errors of the traditional ZUPT algorithm and the foot-to-foot constraint algorithm are 1.4696 and 1.0817 m, and the average errors are 0.8740 and 0.4174 m, respectively. The maximum and average errors of the proposed method are 0.8517 m and 0.3276 m, respectively. Compared with the former two methods, the maximum error of the proposed method is reduced by 42.05 and 21.26%, and the average error of the proposed method is reduced by 62.52 and 21.51%, respectively.

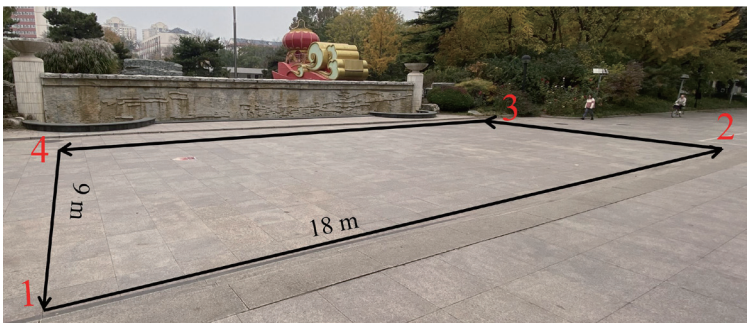


Fig. 4. (Color online) Site of rectangular track experiment.

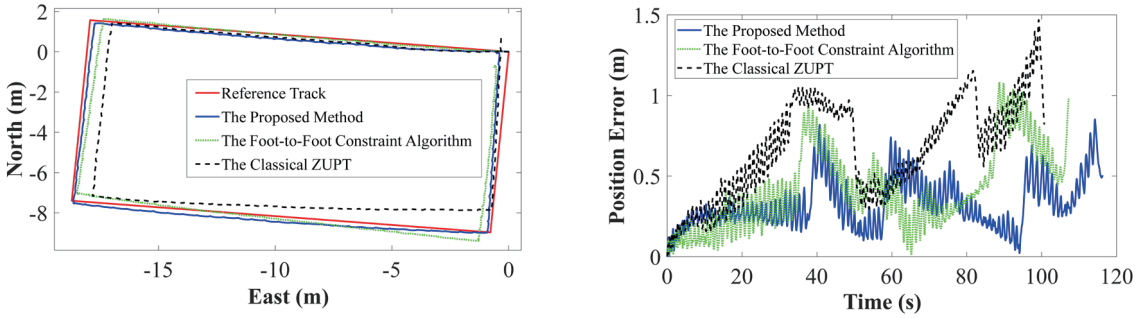


(a) (b)

Fig. 5. (Color online) (a) Track and (b) error curve of the rectangular track experiment.

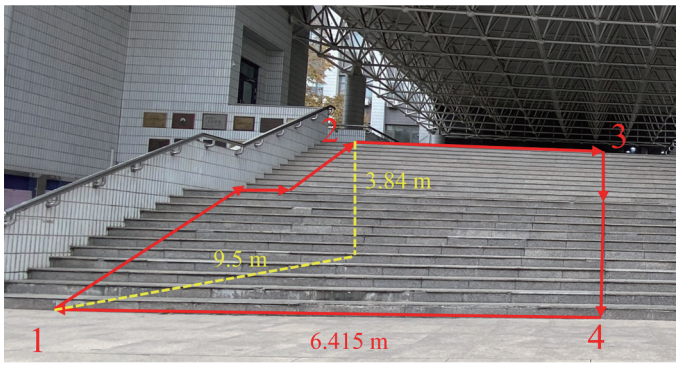


Fig. 6. (Color online) Stair experiment site.

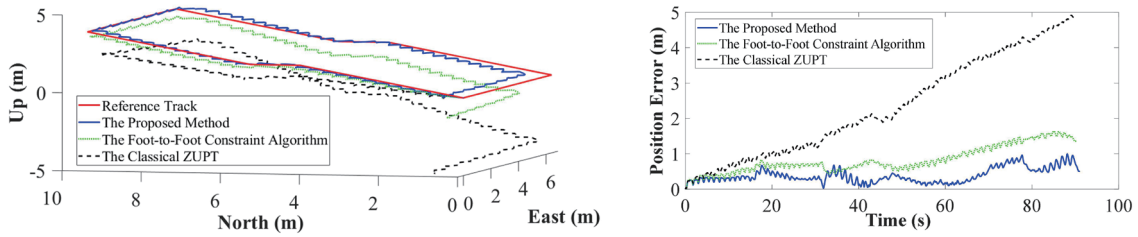


(a) (b)

Fig. 7. (Color online) (a) Track and (b) error curve of the stair experiment.

## (2) Stair experiment

The experimental site consists of 24 steps and a rectangular plane. The length and height of a step are 0.343 and 0.16 m, respectively. The length and width of the rectangular plane measured with a tape are 6.415 and 1.26 m, respectively. Thus, the staircase is 9.5 m long, 6.415 m wide, and 3.84 m high, as shown in Fig. 6. The results are shown in Fig. 7.

The experimental results show that the maximum position errors of the traditional ZUPT algorithm and foot-to-foot algorithm are 4.9159 and 1.6251 m, and the average errors are 2.3265 and 0.8249 m, respectively. The results of the proposed method are 0.9960 and 0.3855 m, respectively. Compared with the former two methods, the maximum error of the proposed method is reduced by 79.74 and 38.71%, and the average error of the proposed method is reduced by 83.43 and 53.27%, respectively.

## 5. Conclusions

A novel pedestrian navigation method based on dual MIMUs was proposed in this work. The dual MIMU only nominally affects the size of the circuit board so it is convenient for pedestrians to wear, and it increased the number of fixed and clear constraints that are not affected by gait and always exist. The use of a linear Kalman filter reduced the computation load and eliminated nonlinear error. Moreover, the SPI-based communication meets the needs of high-speed sampling. Compared with the classical ZUPT and foot-to-foot constraint algorithms, the proposed method had smaller position error and height drift. Moreover, it is more convenient because it can be used in small real-time embedded systems and has high accuracy and small calculation load.

The double MIMU adopted in this work can be extended to three MIMUs without reducing the sampling frequency. Their arrangement on the circuit board can form an equilateral triangle, enabling more information to be obtained. This will be the subject of future research work.

## Acknowledgments

This work was supported by Fundamental Research Funds for the Central Universities (Grant No. 2021ZY68).

## References

1 Y. Zhang: IEEE Access **7** (2019) 61296. https://doi.org/10.1109/ACCESS.2019.2911025
2 K.-Y. Qiu: Sens. Mater. **31** (2019) 3303. https://doi.org/10.18494/SAM.2019.2460
3 S. Youm and K.-S. Shin: Sens. Mater. **33** (2021) 2083. https://doi.org/10.18494/SAM.2021.3303
4 V. Magnago, L. Palopoli, A. Buffi, B. Tellini, A. Motroni, P. Nepa, D. Macii, and D. Fontanelli: IEEE Trans. Instrum. Meas. **69** (2020) 2408. https://doi.org/10.1109/TIM.2019.2960900
5 Y. Wang, D. Vatanparvar, A. Chernyshoff, and A.-M. Shkel: IEEE Sens. Lett. **2** (2018) 1. https://doi.org/10.1109/LSENS.2018.2879315
6 M. Ji, X. Xu, Z. Li, J. Wang, and J. Liu: IEEE Sens. J. **21** (2021) 25649. https://doi.org/10.1109/JSEN.2021.3118388
7 X. Tian, J. Chen, Y. Han, J. Shang, and N. Li: Proc. 2016 35th Chinese Control Conf. (IEEE, 2016) 5325. https://doi.org/10.1109/ChiCC.2016.7554183
8 T. Zhao and A.M. Jalal: IEEE Sens. J. **21** (2021) 13772. https://doi.org/10.1109/JSEN.2021.3070144
9 G. Zheng, W. Qiuying, and Z. Minghui: Proc. 2017 Forum on Cooperative Positioning and Service (IEEE, 2017) 289. https://doi.org/10.1109/CPGPS.2017.8075141
10 X. Wang, S. Yan, D. Li, L. Cao, J. Zhang, Q. Zhang, and X. Zheng: Proc. 2018 IEEE 4th Information Technology and Mechatronics Engineering Conf. (IEEE, 2018) 1786. https://doi.org/10.1109/ITOEC.2018.8740566
11 Y.-L. Hsu, J.-S. Wang, and C.-W. Chang: IEEE Sens. J. **17** (2017) 3193. https://doi.org/10.1109/JSEN.2017.2679138

12 I. Skog, J.-O. Nilsson, and P. Handel: Proc. 2014 IEEE Int. Conf. Electronics, Computing and Communication Technologies (IEEE, 2014) 1. https://doi.org/10.1109/CONECCT.2014.6740346
13 S. Bose, A. K. Gupta, and P. Handel: Proc. 2017 Int. Conf. Indoor Positioning and Indoor Navigation (IEEE, 2017) 1. https://doi.org/10.1109/IPIN.2017.8115944
14 H. Liu, Q. Li, C. Li, and H. Zhao: IEEE Access **8** (2020) 48163 https://doi.org/10.1109/ACCESS.2020.2979484
15 W. Shi, Y. Wang, and Y. Wu: Sensors **17** (2017) 427. https://doi.org/10.3390/s17020427
16 X. Niu, Y. Li, J. Kuang, and P. Zhang: IEEE Sens. J. **19** (2019) 4577. https://doi.org/10.1109/JSEN.2019.2902422
17 H. Zhao, Z. Wang, S. Qiu, Y. Shen, L. Zhang, K. Tang, and F. Giancarlo: IEEE Sens. J. **19** (2019) 8514. https://doi.org/10.1109/JSEN.2018.2866802
18 W. Li, Z. Xiong, Y. Ding, Z. Cao, and Z. Wang: IEEE Access **9** (2021) 42059. https://doi.org/10.1109/ACCESS.2021.3065666
19 Q. Wang, C. Kuang, N. Aboelmagd, K. Liu, X. Cui, and Z. Guo: Proc. 2019 Int. Conf. Communications, Signal Processing, and their Applications (IEEE, 2019) 1. https://doi.org/10.1109/ICCSPA.2019.8713720
20 X. Xu, Y. Sun, X. Tian, L. Zhou, and Y. Li: IEEE Trans. Ind. Electron. **69** (2022) 2055. https://doi.org/10.1109/TIE.2021.3060652
21 Y. S. Suh, Y. S. Ro, and H. J. Kang: IEEE Trans. Instrum. Meas. **61** (2012) 1786. https://doi.org/10.1109/TIM.2011.2181910
22 N. Antigny, M. Serviéres, and V. Renaudin: Proc. 2018 Int. Conf. Indoor Positioning and Indoor Navigation (IEEE, 2018) 206. https://doi.org/10.1109/IPIN.2018.8533680
23 W. Zhang, X. Li, and H. Deng: Proc. 2010 Int. Conf. Intelligent Computation Technology and Automation (IEEE, 2010) 130. https://doi.org/10.1109/ICICTA.2010.385
24 X. Li, Y. Mao, L. Xie, J. Chen, and C. Song: Proc. 2014 IEEE Chinese Guidance, Navigation and Control Conf. (IEEE, 2014) 1760. https://doi.org/10.1109/CGNCC.2014.7007449

## About the Authors

**Shao Chen** received his B.S. degree in mechanical design and manufacturing from Beijing Forestry University in 1984 and his Ph.D. degree in mechanical design and theory from 2007. He is currently an associate professor at the School of Technology, Beijing Forestry University. His research interests include pedestrian inertial navigation and forest fire fighting technology.
(chenshao@bjfu.edu.cn)

**Zhenchun Lu** received his bachelor's degree in automation from Northeastern University in 2019. He is currently studying control engineering at Beijing Forestry University. His current research field is pedestrian inertial navigation systems based on MEMS sensors.
(lzcneu2018@163.com)

**Xiangbo Xu** received his B.S. degree from Shandong University in 2006 and his Ph.D. degree in precision instruments and machinery from Beijing University of Aeronautics and Astronautics in 2014. He is currently an associate professor at the School of Technology, Beijing Forestry University. His research interests include pedestrian inertial navigation and permanent magnet motor control in high-speed rotating machinery.
(xuxiangbo@bjfu.edu.cn)

**Jinhao Liu** received his B.S. degree in mechanization of harvesting and transportation and his Ph.D. degree in forest engineering from Northeast Forestry University, Harbin, China, in 1982 and 2003, respectively. He is currently a professor at the School of Technology, Beijing Forestry University, Beijing, China. His research interests include pedestrian inertial navigation and special robots. (liujinhao@bjfu.edu.cn)

**Zhongwei Bi** received his B.S. degree from Inner Mongolia University of Science & Technology in 2012 and his M.S. degree in mechanical engineering from Shandong University in 2015. He is currently an engineer at Beijing High Speed Suspension Power Technology Co., Ltd. His research interests include magnetic bearings, high-speed permanent magnet motors, and pedestrian inertial navigation. (bizhongwei@126.com)